Sand ripples under water with complex wave motion

K. Scheibye-Knudsen, C. Ellegaard, and F. Bundgaard*
Niels Bohr Institute, Blegdamsvej 17, DK-2100 Copenhagen, Denmark

Thomas Sams
Danish Defense Research Establishment, P. O. Box 2715, Ryvangs Alle 1, DK-2100 Copenhagen, Denmark
(Received 27 February 2004; revised manuscript received 21 June 2004; published 15 July 2005)

Experiments studying ripple formation under water have usually used sinusoidal driving force. Here an experiment is presented where the driving force can be an arbitrary wave form, thus trying to mimic the realistic wave motion in shallow water coastal zones. We study a simple modulated sine wave and more complicated wave forms with several superposed harmonics. In particular we demonstrate how a small higher order harmonic can have a dramatic effect on the wavelength of the ripple pattern.

DOI: 10.1103/PhysRevE.72.016209 PACS number(s): 89.75.Kd, 47.54.+r, 45.70.Qj, 47.32.Cc

I. INTRODUCTION

The characteristic ripple patterns seen in the sand at the beach where waves come rolling in fascinate many. Scientific studies of ripples have been going on since Ayrton's first qualitative studies in 1904 [1], and Bagnold's first quantitative measurements in 1946 [2].

Bagnold found that above a certain threshold a sandbed is unstable and initially forms so-called *rolling grain ripples*, which grow into fully developed *vortex ripples* (though sometimes with a long transient). The vortex ripples are so named because they are created by the vortex on the lee side of the ripple. The reversed flow due to this vortex will push sand grains toward the crest of the ripple, causing it to grow until it reaches a slope where avalanches begin to occur on the ripple sides. Therefore the size and shape of the vortex ripple depend on the equilibrium between the shear from the vortex and the destabilizing avalanches.

More recent experiments have further probed the structure of the ripples and the dynamics which govern them [3–5]. Generally, there is a linear relation between the amplitude of the motion of the waves and the wavelength of the ripple pattern [6], where the wavelength is approximately 0.6 times the peak-to-peak amplitude of the drive.

However, all these previous experiments have used a simple form of driving, namely, a "pure" sinusoidal drive, which corresponds to the current created at the bottom of ideal surface waves. While it is easy to create such a form of driving, it does not give a realistic image of the processes that govern ripple formation on sandbeds. In a natural environment real waves come as a mix of different sizes and frequencies [7–9], and are thus far from ideal, perfectly periodic waves [see especially Chap. 2 (10) in [9]]. Because the different wave sizes individually set a preferred length scale, it is not known how the wavelength of the ripple pattern depends on the different wave amplitudes.

The present paper is a study of the dynamics that govern ripple formation when the driving is nonideal. We study the patterns formed by ripples when the driving is not a "pure" sine wave, but instead a more complicated motion consisting of superposed sine waves. This looks more like natural waves, as it consist of strokes of several different sizes.

The results from these experiments are generally consistent with earlier results, but only when a suitable definition of the driving amplitude is used, since the amplitude in our experiments is nonunique. At the same time it is found that the ripple patterns can be very sensitive to small changes in the details of the driving, causing large differences in the ripple pattern for driving with almost identical parameters.

Section II describes the experimental setup. In Sec. III the results from experiments using driving with several different strokes are presented, while Secs. IV and V present results from experiments where small changes in driving parameters change the resulting ripple pattern greatly.

II. EXPERIMENTAL SETUP AND CONSIDERATIONS

The present study has been carried out using a setup much like the one used originally by Bagnold, where a tray filled with sand is oscillated back and forth under still water. This is advantageous for purely mechanical reasons. The tray weighs much less than the surrounding water making it easier to move the tray rather than moving the water. This introduces inertial forces into the grain dynamics, but in the regime studied they have negligible effect on the ripple shape and pattern wavelength, as explained in Sec. V A.

A sketch of the experimental setup is shown in Fig. 1. The tray is an aluminum plate 0.5×1 m^2 and 5 mm thick. It is suspended from an aluminum frame in a water filled tank of sufficient size to avoid effects from the sides of the tank. To confine the sand to the aluminum plate straight aluminum segments have been placed along the edges. The edges perpendicular to the motion have been rounded to minimize the vortices made when oscillating the tray, and a gently inclining slope makes a smooth transition between the edge and the sand (see Fig. 1).

The sand is an approximately 2 cm thick layer of spherical glass beads, 250–350 μm in diameter. Before each experiment the sediment is stirred and smoothed, producing a flat sandbed. On top of the tank a 3 cm thick plexiglass plate is placed to prevent sloshing and surface waves from interfering with the study of the ripple patterns. An eight-bit 1024×1024 pixel Dalsa gray scale charge-coupled device

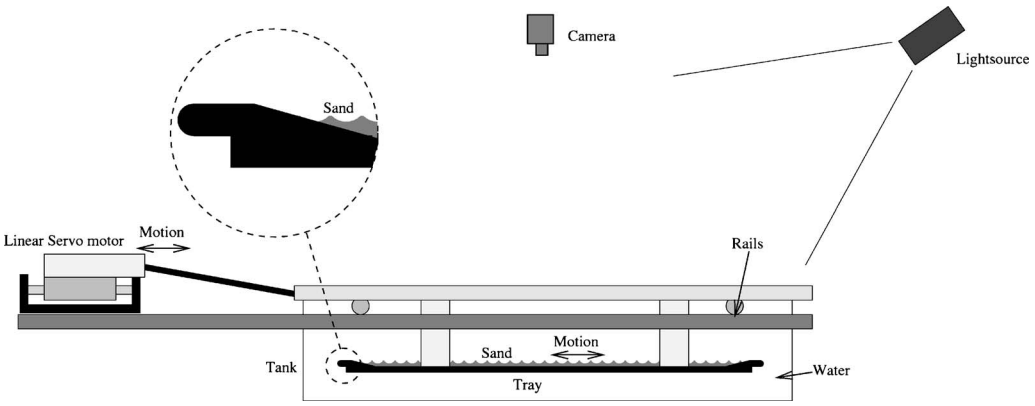

FIG. 1. Sketch of the experimental setup. The tray filled with sand is driven back and forth in the water, while a digital camera is used to take pictures of the developing ripple pattern.

camera is placed above the water tank and used to record images of the ripple pattern as it evolves. A 500 W spotlight illuminates the ripple pattern from one side to produce a contrast-rich image.

The ripple pattern wavelength λ is extracted from the images taken by the camera as the most common distance between two neighboring ripple crests. The ripple wavelength would be nearly uniform (barring small areas with defects) with a difference in wavelength of different parts of the pattern of about 3 mm (compared to the wavelengths of 4–10 cm).

The motor driving the tray is a Thrusttube linear servo motor controlled by an Elmo digital controller. By using these it is possible to program the movement of the sand tray in (almost) any complex oscillatory back-and-forth motion, with only a minute discrepancy from the programmed motion caused by random noise.

A few experiments were performed with a different experimental setup. The differences are that a narrow channel (1 cm) is used instead of the wide tray and that the setup is made of plexiglass. The setup is in this way practically one dimensional, where the usual two dimensional features (defects, brick patterns, etc.) are absent. The advantages to this setup are that the ripples can be observed from the side and that the tank and the water are light enough to make it feasible to move water instead of moving the sand tray itself. The same linear servo motor was moved to this setup and used to drive the system.

In general the system is driven at frequencies and amplitudes that give a (ripple) Reynolds number of 1000–6000 and a Shields parameter of roughly 0.1–0.2 (see [10] for a more detailed discussion).

Driving equations

In this study we have concentrated on periodic forms of motion. Any periodic function can be expressed as a Fourier sum of sinefunctions:

$$x(t) = \sum_{n=0}^{\infty} a_n \sin(n\omega t + \phi_n). \tag{1}$$

However, due to the nonlinear dynamics of the vortex, any motion where the strokes have different lengths in opposite directions will induce a drift in the ripple pattern. In order to avoid this drift, the motion is constructed from only the odd harmonics, which have the desired symmetry properties.

The majority of the experiments were made with only the two lowest orders of the superpositions, that is,

$$x(t) = a_1 \sin(\omega t) + a_3 \sin(3\omega t + \phi) \tag{2}$$

where x is the position of the tray.

Depending on the values of the parameters a_1, a_3, and ϕ the total periodic motion consists of strokes of different sizes, where we define the stroke size as the distance from a local maximum to the following minimum, and vice versa. Figure 2 shows a typical motion where the stroke sizes are marked.

Two other types of motion were also studied. These were

$$x(t) = a_4 \sin(4\omega t) + a_5 \sin(5\omega t + \phi), \tag{3}$$

$$x(t) = A \sin(\omega t)\left[1 + B \sin\left(\frac{\omega t}{5}\right)\right]. \tag{4}$$

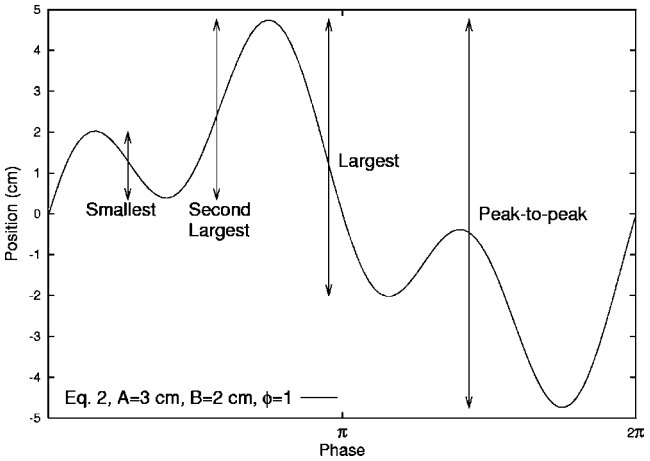

FIG. 2. Equation (2) here the four stroke sizes are marked; the parameters are a_1=3 cm, a_3=2 cm w and ϕ=1.

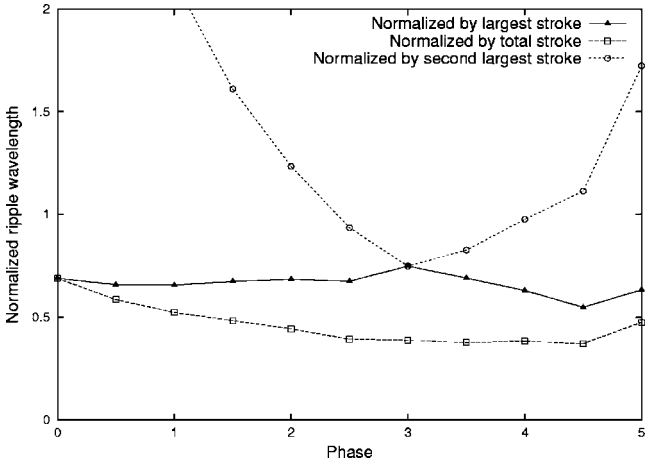

FIG. 3. The rescaled wavelength as a function of phase. The driving motion uses Eq. (2) with parameters $a_1=3$ cm, $a_3=1$ cm. The lines are merely a guide to the eye to connect points with the same rescaling.

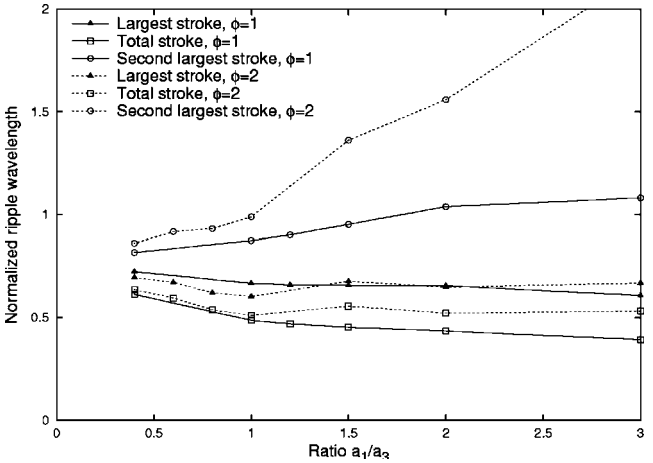

FIG. 4. The data from experiments using Eq. (2) with $\phi=1$ (solid) and $\phi=2$ (dotted); the normalized ripple wavelength is plotted as a function of the ratio a_1/a_3. The wavelength is scaled using three length scales, the largest stroke (▲), the next largest stroke (○), and the total peak-to-peak stroke (□).

These are essentially slowly modulated sine waves and are not symmetric. However, the asymmetry is small and the drift is not very pronounced.

III. RESULTS

In this section the data obtained by using the driving presented previously will be analyzed. We will start with the simplest forms of motion, that is, those governed by Eq. (2), and present data obtained for different values of the parameters, and thereafter present the data obtained from the more complicated driving [Eqs. (3) and (4)].

A. Ripple formation with first and third harmonics

With the driving motion governed by Eq. (2) we vary all the parameters separately.

We changed the parameters either by keeping a_1 and a_3 constant and changing the phase, or by keeping the phase constant and changing the ratio between a_1 and a_3.

For the experiment with constant ratio, a_1 was kept at 3 cm and a_3 was 1 cm. The phase was varied from 0 to 5 in increments of 0.5. The experiments were run for roughly half an hour from a flat sandbed after which the ripple wavelength was recorded. With a frequency of 0.7 Hz, this was enough to ensure that the patterns had stabilized.

According to previous experiments we would expect that the ripple wavelength is linearly dependent on the length scale defined by the amplitude of the motion. In this series of experiments, one can (for most values of ϕ) define four length scales: the maximum peak-to-peak distance and three different stroke sizes (see Fig. 2). To probe how the final ripple wave-length depends on the different stroke sizes we rescale the wavelength (λ) with the relevant stroke size in the following manner:

$$\lambda' = \frac{\lambda}{S_x}, \tag{5}$$

where S_x is one of the stroke sizes defined by the motion (see Fig. 2) and λ' is the rescaled wavelength.

The rescaled wavelength is shown in Fig. 3. The best collapse (meaning λ' constant) of the data is found when the wavelength is scaled by the largest stroke. The rescaled wavelength is consistent with previous experiments using the same setup ($\lambda \approx 0.6 S_x$) [10]. We have chosen not to show the points for the wavelength normalized by the smallest stroke size, as these lie far outside the region displayed, and show no meaningful collapse.

In the second part of the experiments the phase was kept constant for each experimental series, and the ratio between a_1 and a_3 was varied between 0.4 and 3. The values of ϕ were 0, 1, 2, and π, while a_1 and a_3 ran from 1 to 3 cm. The amplitudes of the two harmonics were then varied for each of the different phases, and the final wavelength was found. The following part deals with the first three cases, while the last ($\phi=\pi$) is described separately in Sec. IV, since we concentrated on a different aspect of the pattern formation with these experiments.

The two most interesting experiments are the ones with ϕ of 1 and 2, as the driving in these cases gives four different length scales. The normalized results for these two experiments are shown in Fig. 4. Again the best collapse is found when the wavelength is normalized by the largest stroke size, and is consistent with previous results.

In the experiment with $\phi=0$, the motion consists of a large stroke from one extreme to another and a smaller oscillation around the extreme. Therefore only two different length scales can be naturally defined from the motion, and when normalized by the largest stroke, the wavelength falls again in the regime of earlier experiments. The results are shown in Fig. 6 below, together with the rest of the data.

B. Ripple formation with modulated waves

With the driving described by Eqs. (3) and (4), many stroke sizes are present and thus the final wavelength could

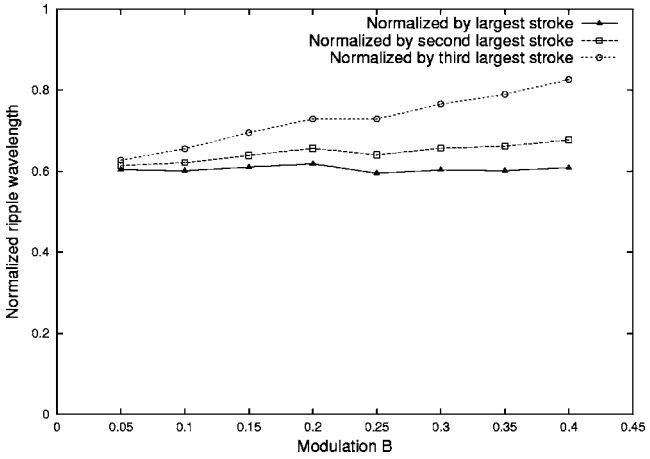

FIG. 5. The data from runs using Eq. (4) with $A=4$ cm. The normalized ripple wavelength is scaled by the largest stroke (▲), the second largest stroke (□), and the third largest stroke (○).

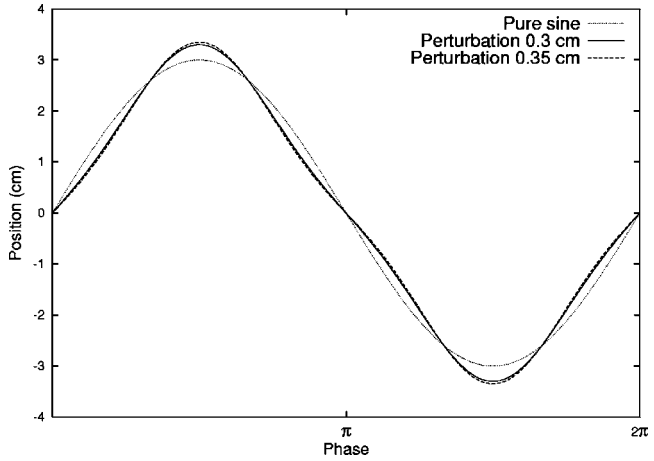

FIG. 7. The position during one period of motion using Eq. (2). The lines (though hard to distinguish) correspond to motions which consistently create a ripple pattern with either a large wavelength (solid) or a small wavelength (dashed). A pure sine wave is shown for comparison (dotted).

depend on any of these different length scales. In the experiment with the motion described by Eq. (3) with $\phi=0$, the parameters a_4 and a_5 were varied from 1.5 to 3.0 cm (probing a ratio between 0.5 and 2). In the experiments using Eq. (4) A was set to 4 cm and the modulation (B) was between 0.05 and 0.4.

Figure 5 shows the dependence of the final rescaled wavelength as a function of the modulation for experiments using Eq. (4). It is clear that the final wavelength is linearly dependent on the length scale of the largest stroke, while the second largest stroke gives a poorer scaling. It is also seen that the final rescaled wavelength is independent of the modulation.

The data from the experiments using Eq. (3) are shown together with the rest of the results in Fig. 6, again scaled by the size of the largest stroke.

IV. PERTURBED SINE DRIVING

In the case of Eq. (2) with the phase $\phi=\pi$, we concentrated on another aspect of ripple formation. We used a "perturbed sine" wave, that is, we used a form of driving where the amplitude a_1 was much greater than a_3; this generates a driving force looking as if it has the same characteristics as a pure sine drive, except for a small deviation near the middle of the stroke.

The effect of the deviation was investigated by holding a_1 constant at 3 cm and decreasing a_3 in small steps (from about 0.5 cm). We found a sharp transition between ripple patterns with wavelength corresponding to the total stroke size, and ripple patterns with about half that wavelength. The transition takes place at a value of the parameter a_3 where there is no visible turning point, but only a slight "hesitation" during the middle of the stroke. In Fig. 7 the position is shown for parameter values just above and just below the transition.

This was further probed in a series of experiments where the parameter a_1 was held constant at 3 cm, and the final

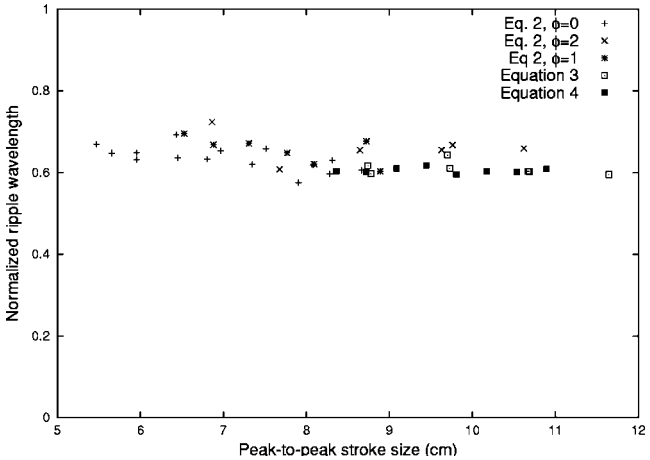

FIG. 6. The normalized wavelength as a function of the total peak-to-peak size. The wavelength is scaled by the size of the largest stroke.

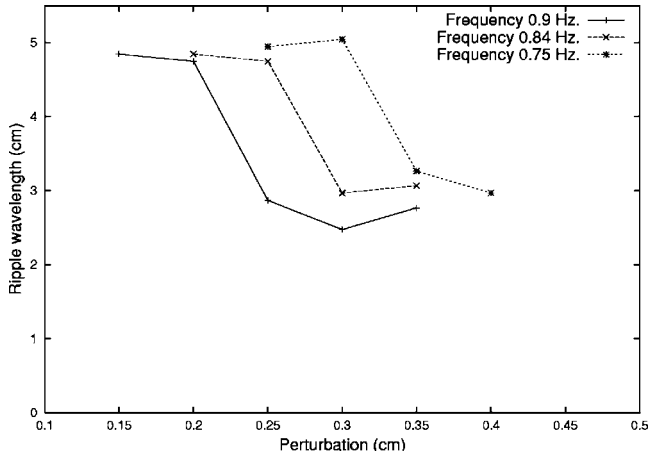

FIG. 8. The final wavelength as a function of the size of the perturbation [a_3 in Eq. (2)], for $a_1=3$ cm and $\phi=\pi$, in the two dimensional setup.

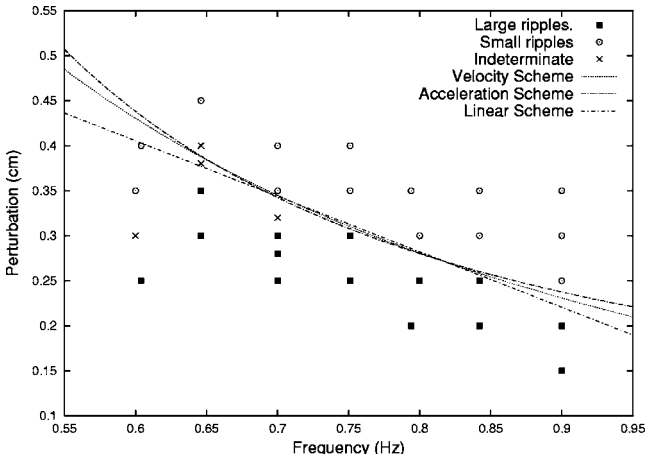

FIG. 9. The phase space showing whether the final ripple pattern has a large (4–5 cm) or small (2–3 cm) wavelength. The parameter a_1 was kept constant at 3 cm during these experiments. The lines corresponds to different schemes for how the transition scales (see text).

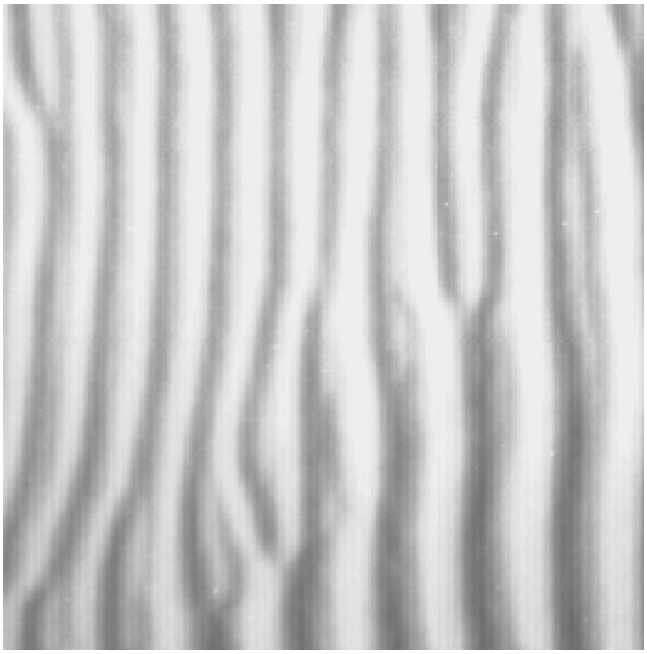

FIG. 10. Picture of a ripple pattern with patches with large wavelength and patches with small wavelength.

ripple pattern was recorded for different values of the parameter a_3 and different frequencies. It was found that when the value of a_3 was decreased below a certain point the final wavelength suddenly shifted from a ripple pattern with a rather small wavelength (2–3 cm) to a ripple pattern with a large wavelength (4–5 cm). We found that this transition also depends on the frequency of the driving. Some examples of this can be seen in Fig. 8, while the results are summarized in Fig. 9, showing that for smaller frequencies the perturbation needed to create the small ripple pattern is greater. The points around 0.6 Hz deviate from the other data points; this is probably due to the extremely slow dynamics at this frequency (just above the threshold for grain motion). The indeterminate points represent ripple patterns where large wavelength areas coexist with areas with small wavelength. An example of this is shown in Fig. 10. The patterns persisted even after more than one day of continuous oscillation.

The lines in Fig. 9 are fits to the midway point between the lowest data point with small ripple wavelength and the highest data point with large ripples for each frequency. The different functions correspond to various schemes for the transition's dependency on the perturbation and frequency. If the transition depended on an absolute change in acceleration from a pure sine wave, $a_3\omega^2$ should be constant, while $a_3\omega$ should be constant if the transition depended on an absolute change in velocity.

Another possibility is that the transition is the consequence of a relative change in the motion from a pure sine wave. This would mean that a_3 should be constant with no dependence on the frequency, but if the transition depended

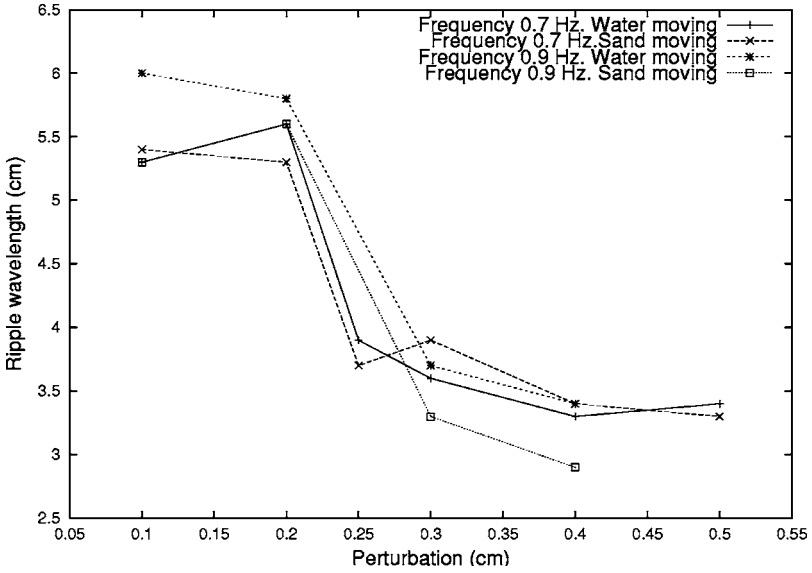

FIG. 11. The final wavelength as a function of the size of the perturbation [a_3 in Eq. (2)], for $a_1=3$ cm and $\phi=\pi$, in the one dimensional setup, showing both situations where the sand is moved and the water is moved.

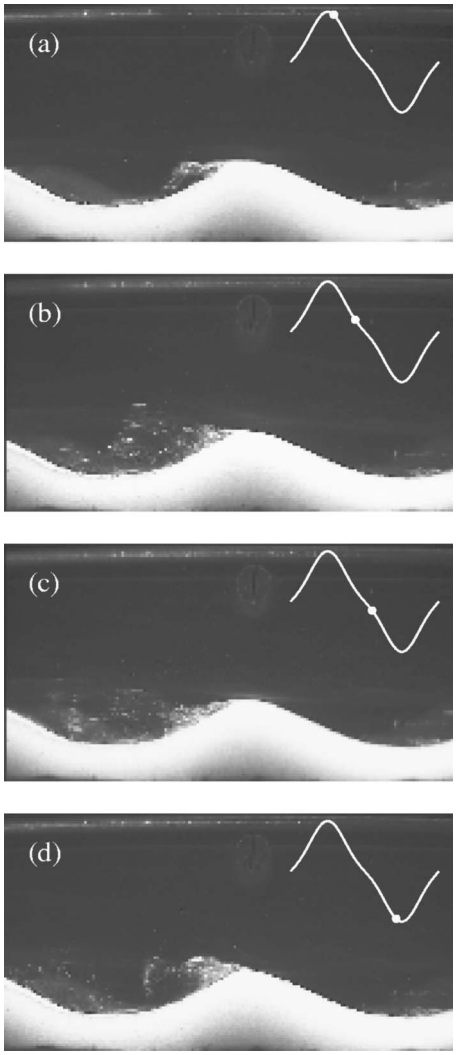

FIG. 12. Images showing how the vortices are created and shed, due to the perturbation of the pure sine wave. The overall flow is from right to left. The insets show approximately at what point in the motion the pictures are taken. The pictures show the vortex growing behind the ripple (a) and (b), the vortex detaching from the side of the ripple (c), and a new vortex forming behind the ripple while the old vortex travels downstream (d).

on a relative change *and* how fast this change occurred the linear relation should be expected. As can be seen none of these possibilities are excluded by the data.

Figure 8 shows the abruptness of the transition between large wavelength and small wavelength ripple patterns. We find that the change in a_3 of only 0.5 mm (compared to a total stroke of $\approx$3.3 cm) is enough to change the final wavelength from $\approx$5 cm to $\approx$2.5 cm. This small change of the motion is imperceptible to the naked eye, and the fact that it generates such a pronounced change is remarkable.

We have examined this transition only at $\phi=\pi$, but it should also be possible to observe it at other values of the phase. However, for geometrical reasons it should be most pronounced when the deceleration happens at the midpoint of the stroke.

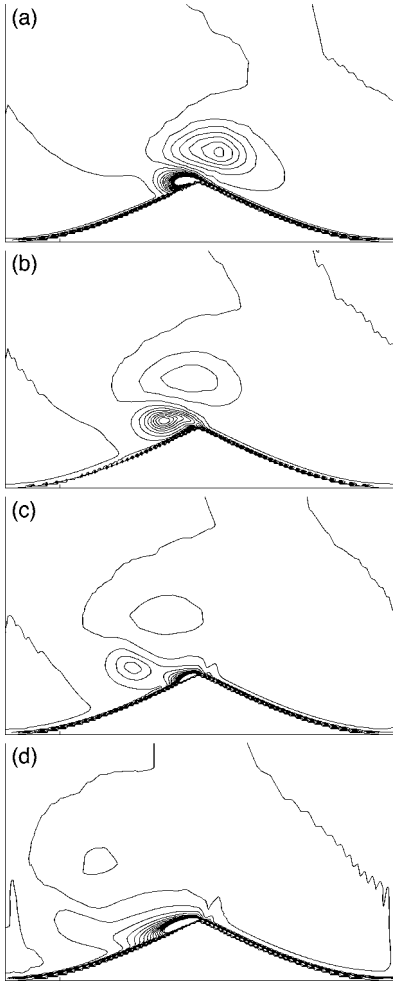

FIG. 13. Images from a numerical simulation with DUNE2D [11], plotting the contours of the vorticity field at different times during the half cycle. The images show the evolution of the vortex, and correspond roughly to the pictures in Fig. 12.

V. SIDE VIEW SETUP

Since the wavelength of the ripple pattern depends primarily on the size of the vortex created on the lee side, it is evident that the changes in the pattern stem from alterations in the vortex size and dynamics. The study of the vortex was performed in the one dimensional setup.

A. Inertial effects

Because the setup is light enough to make it possible to move the water instead of the sand, the influence of inertia on ripple generation and dynamics can be examined.

Probing the inertial effect was performed using a perturbed sine wave, that is, Eq. (2) with only a small third order component compared to the prime driving amplitude. Since the changes in pattern wavelength are very dramatic, the possible consequences of inertial effects would probably be most noticeable with this type of motion.

We performed two experimental series at two frequencies with this setup, one where the water was oscillated back and forth, and one where the sand was oscillated. The system was

oscillated at a frequency of 0.7 and 0.9 Hz, and a_3 was from 0.1 to 0.5 cm.

The results are shown in Fig. 11. It is seen that the differences in the way the system is driven have very little influence on the wavelength of the ripple pattern. Even though the transition appears at a smaller value of $a_3(a_3 \sim 0.2$ cm) than for the two dimensional system ($a_3 \sim 0.3$ cm) at 0.7 Hz, the fact that the data are very similar for both types of driving suggests, that the inertial effects are negligible. It should be noted that though the wavelengths are similar for the 0.9 Hz base frequency, the system takes longer to stabilize in this case and the pattern is somewhat less regular, which suggest that we are at the point where the inertial effects begin to play a part in the dynamics (acceleration ~ 2 m s^{-2}).

It also appears that the ripple pattern wavelength in general is greater than for the two dimensional system, but since this is evident for both types of driving, it is more likely to be an effect of the narrow channel in this setup.

B. Visualizing the flow

To gain insight into the dynamics of the vortex, and especially what happens when crossing from large to small pattern behavior, we wanted to observe the vortex itself.

In order to visualize the dynamics of the vortices we seeded the flow with Irodin 100 silver pearl, which is a powder consisting of small (10–25 μm) reflective scales, and used a standard digital video camera to record the dynamics of the vortex.

In Fig. 12 four frames from one half cycle show the flow above the ripple. The vortex forms on the lee side of the crest (a), then grows (b), but when the motion decelerates slightly during the middle of the stroke, the vortex detaches from the crest (c) and a new vortex forms on the lee side, while the old vortex travels downstream (d).

While the images recorded indicate that the vortex is broken up in some way, they do not show this very clearly and do not show exactly the same vortex from stroke to stroke because the flow is turbulent. Therefore we tried to see if the numerical simulation program DUNE2D [11] could capture the average features of the flow in this situation. DUNE2D solves an averaged version of the Navier-Stokes equation, and was created by Tjerry [11]. It has been used by Andersen [12] for extracting the selected ripple wavelength under sinusoidal flow. As seen in 13, the simulation captures essentially the same features as seen in the experiment (Fig. 12).

The simulation clearly shows how the vortex forms and is shed from the crest before moving downstream. In (a) a vortex begins to form on the left hand side of the ripple, while the old vortex from the previous half cycle is ejected from the ripple and passes over the crest (this has previously been observed [3]). The vortex continues to grow (b). Then the vortex detaches from the ripple and begins to move downstream, while a new vortex begins to form on the side of the ripple (c). The old vortex is carried further downstream and broken up, while the newly formed vortex grows (d), until the flow reverses and the vortex is ejected back across the crest.

Summing up, the "hesitation" causes the vortex to be shed from the ripple, thereby preventing the vortex from growing to the size it would otherwise obtain.

The agreement between the experiments and the numerical simulation is striking and clearly shows that the separation bubble can be detached from the generating structure by very small changes in the overall flow.

VI. CONCLUSION

We have studied ripple formation under water under conditions that resemble natural waves more than the usual (in a laboratory) sinusoidal motion. *A priori* the generated ripple wavelength could have depended on the average, the total, or some other function of the driving wavelengths.

The main result of these experiments is that the selected wavelength for complex driving motion is determined by the largest single stroke and not by the total excursion, nor is it influenced in any significant way by the other strokes. A small stroke creates only a small vortex behind a ripple and since the size of the vortex determines where sand is deposited on a ripple, a small vortex will deposit sand on the side of a larger ripple. Later, when a larger vortex forms behind the ripple the vortex will extend beyond the area that was covered by the small vortex, and scour the deposited sand away.

The details of what elements of the motion set the stroke size are more surprising. In Fig. 2 the definition is obvious. In the experiment, however, it turns out that a well-defined extremum is not necessary. Just a slight decrease in the velocity is enough to effectively split the stroke in two. It has been shown, both by visual inspection and by numerical simulation, that the effect of the slowing down is a detachment and shedding of the vortex, after which a new vortex is created. Both vortices are smaller than the vortex produced without the slowdown. In the case of the phase $\phi = \pi$, the new size of the vortex is about half of what it would be without the slowdown, resulting in a ripple wavelength of approximately half of the wavelength with no perturbation.

It is surprising indeed that the transition is so abrupt: a change of only 0.5 mm relative to the 30 mm of a_1 which determines the full stroke.

ACKNOWLEDGMENTS

The authors would like to thank Tomas Bohr and Ken Haste Andersen for useful discussions and input. This work was supported by the Danish Natural Science Research Council.

[1] H. Ayrton, Proc. R. Soc. London, Ser. A **84**, 285(1910).
[2] R. Bagnold, Proc. R. Soc. London, Ser. A **187**, 1 (1946).
[3] M. A. Scherer, F. Melo, and M. Marder, Phys. Fluids **11**, 58 (1999).
[4] A. Stegner and J. Wesfreid, Phys. Rev. E **60**, R3487 (1999).
[5] J. L. Hansen, M. v. Hecke, C. Ellegaard, K. H. Andersen, T. Bohr, A. Haaning, and T. Sams, Phys. Rev. Lett. **87**, 204301 (2001).
[6] P. Nielsen, J. Geophys. Res., C: Oceans Atmos. **86**, 6467 (1981).
[7] J. Falnes, *Ocean Waves and Oscillating Systems* (Cambridge University Press, Cambridge, U.K., 2002).
[8] I. Lavrenov, *Wind-Waves in Oceans* (Springer, Berlin, 2003).
[9] I. Young, *Wind Generated Ocean Waves* (Elsevier, Amsterdam, 1999).
[10] J. L. Hansen, Ph.D. thesis, Niels Bohr Institute, 2001, available at www.nbi.dk/~lundbek
[11] S. Tjerry, Ph.D. thesis, ISVA, Technical University of Denmark, 1995.
[12] K. Andersen, Ph.D. thesis, Niels Bohr Institute, 1999, available at www.nbi.dk/~kenand